Electrochimica Acta 393 (2021) 139019

Contents lists available at ScienceDirect

Electrochimica Acta

journal homepage: www.elsevier.com/locate/electacta

The rate-determining term of electrocatalytic reactions with first-order kinetics ☆

Jun Huang [a,b,*], Xinwei Zhu [a], Michael Eikerling [a,c,*]

[a] Forschungszentrum Jülich GmbH, Institute of Energy and Climate Research, Theory and Computation of Energy Materials (IEK-13), Jülich 52425, Germany
[b] Institute of Theoretical Chemistry, Ulm University, Ulm 89069, Germany
[c] Jülich Aachen Research Alliance: JARA-Energy, Jülich 52425, Germany

ARTICLE INFO

Article history:
Received 5 June 2021
Revised 22 July 2021
Accepted 28 July 2021
Available online 4 August 2021

Keywords:
Electrocatalytic reactions
Electrochemical kinetics
Tafel slope
Volcano plot
Targeted design of catalysts
Microkinetic modeling

ABSTRACT

The quest to find highly active electrocatalysts for electrochemical energy conversion devices requires mechanistic concepts to guide activity analysis, the most commonly employed ones being the rate-determining step (RDS) and the potential-determining step (PDS). Here we present a generalized concept, the rate-determining term (RDT). The RDT concept is not simply a semantic change but a nontrivial improvement over the RDS and PDS concepts, as it incorporates the detailed kinetics and thermodynamics of multistep electrocatalytic reactions. The theoretical basis of the RDT concept is steady-state microkinetic modelling, for which we put forward a unified and compact formalism for electrocatalytic reactions with first-order kinetics. The new formalism allows us to write the expression for the rate determining term of the reaction in general and analytical form. The RDT concept is then used to derive analytical expressions for the Tafel slope and the volcano plot of activity that can be used in the studies of multistep electrocatalytic reactions. Thereafter, the efficacy of the RDT concept is demonstrated for two important case studies, the oxygen evolution reaction and the carbon dioxide reduction reaction. Fundamental insights into the origins of the potential-dependent Tafel slope are obtained. An important consequence, gleaned from this analysis, is that one cannot infer a RDS from measured Tafel slopes. In addition, kinetic factors are shown to exert a notable influence on the slopes and apex location in volcano plots of activity. The present RDT is anticipated to be a powerful analytical tool for multistep electrocatalytic reactions with first-order kinetics.

1. Introduction

Electrochemical energy conversion is concerned with emerging technologies that are important for a sustainable energy ecosystem, including polymer electrolyte fuel cells, water electrolysers and carbon dioxide reduction cells [1,2]. Electrocatalysis is for electrochemical energy conversion what semiconductor physics has been for computer and information science: the key scientific discipline to yield breakthrough progress in technology development. Compared with other types of electrochemical reactions, electrocatalytic reactions are characterized by a strong dependence of the activity on the properties of the electrode material [3–5]. Current research efforts thus strive to unravel the impact of atomic composition, crystalline structure, electronic structure and surface configuration of the catalyst on the electrocatalytic activity [3,5–6]. This understanding is crucial to guide materials screening and bolster materials design in order to find electrocatalysts that are highly active towards the particular reaction under consideration [7–8].

Except simple chemisorption reactions, such as halide absorption [4], most electrocatalytic reactions proceed via multiple elementary steps and involve several intermediates adsorbed on the electrode surface. To make life easier, it is seemingly intuitive to identify an elementary step that determines the net rate of the overall reaction. Two types of “determining step” have been considered in the field for decades. One is the rate-determining step (RDS), a well-established concept borrowed from chemical kinetics [9,10]. The other is the potential-determining step (PDS), a concept specifically conceived for electrocatalysis [6–14].

☆ Dedicated to the memory of Sergio Trasatti, who continues to inspire scientists in electrocatalysis.

* Corresponding authors at: Forschungszentrum Jülich GmbH, Institute of Energy and Climate Research, Theory and Computation of Energy Materials (IEK-13), Jülich 52425, Germany.

E-mail addresses: jhuangelectrochem@qq.com (J. Huang), m.eikerling@fz-juelich.de (M. Eikerling).

https://doi.org/10.1016/j.electacta.2021.139019

PDS is the elementary step with the most positive Gibbs reaction free energy. It is then the last step to become exergonic when the imposed overpotential is increased. The minimal overpotential required to render the overall free energy profile downhill (without considering activation barriers) is termed the thermodynamic overpotential [11,14,15]. The PDS and associated thermodynamic overpotential are readily identified from the free energy profile calculated, most often, from density functional theory (DFT). In the literature, a well-documented example is the oxygen reduction reaction (ORR) [16,17]. For the ORR at the most active pure metal, that is Pt, the PDS corresponds to the desorption of OH_{ad}, $OH_{ad} + H^+ + e \rightarrow H_2O$, and the onset potential of ORR current is ca. 0.9 V_{RHE}; only below this potential does the change in Gibbs energy of the PDS become negative. This PDS is the reason that Pt is found on the left rising flank of the ORR volcano curve, which indicates a process inhibited by too strong binding of intermediates or product species. In the PDS method, all complications that arise when detailed kinetic analyses have to be conducted vanish and simple thermodynamic reasoning is used to guide catalyst design. The PDS concept has been widely employed with success, see review articles [15–17].

However, counterexamples also exist in literature, which are not surprising, considering the simplicity of the PDS concept. Gómez-Marín et al. reported the sequence Pt(211) > Pt(110) > Pt(111) > Pt(100) for the ORR activity at 0.9 V_{RHE} in acidic solution, contradicting the sequence Pt(111) ≫ Pt(100) ≫ Pt(110) > Pt(211) given by PDS-based theoretical results [18]. Recently, Zhou et al. measured a sequence Ir(111) < Rh(111) < Pt(111) for the ORR in acidic solution, while the PDS concept predicts a sequence Rh(111) < Ir(111) < Pt(111) [19]. More counterexamples include chlorine evolution at RuO_2(110) according to Exner and Over [20], and a hypothetical case proposed by Koper [14]. Chen et al. argued that the PDS method may lead to inaccurate, even qualitatively wrong, results near the volcano apex [21]. In subsequent improvements, the PDS method has been augmented by adding kinetic considerations to it, e.g., by Hansen et al. [22], Huang et al. [23], Chen et al. [21]. and Exner [24].

The RDS is the prevailing concept used in analyzing multistep reactions. It rests upon two major assumptions[1] [10,25]. First, a slow step must exist that controls the net rate of the overall reaction, whereas all other steps are in quasi-equilibrium, namely their forward and backward reaction rates are so large that they are nearly equal, relative to the rate of the slow step. Second, the reaction surface must be void of adsorbed intermediates. The RDS concept has been extensively and controversially discussed in the field of heterogeneous catalysis, see Campbell [26], Dumesic [27], Bockris and Nagy [25], Kozuch and Martin [10], and Koper [14]. Many alternative concepts have been developed, such as Dumesic's lowest reversibility [28], Stegelmann's et al. degree of rate control [29], and Kozuch and Martin's rate-determining states [10]. When applied to electrocatalytic reactions, the main deficiency of the RDS concept stems from the second assumption. For example, Shinagawa et al. demonstrated [30], using the hydrogen evolution reaction (HER) as an example, that the usual argument that a Tafel slope of 120 mV dec^{-1} indicates the Volmer step as the RDS of the HER is erroneous, because this value of the Tafel slope may well be obtained with the Heyrovsky step as the RDS with a high coverage of adsorbed hydrogen. Coverage- and potential-dependent Tafel slopes have been observed and investigated by many authors, see, for example, Refs. [21,23,24,30,31].

For an accurate mechanistic analysis of electrocatalytic reactions, the consideration of potential-dependent coverages of adsorbed intermediates is important. Detailed microkinetic modelling is usually needed to perform this analysis; however, such an approach is usually considered prohibitive due to the mathematical treatment involved [32]. The energetic span model (ESM), developed by Kozuch and Shaik and lucidly elucidated in Ref. [33], is a simple yet viable approach to describe potential-dependent coverages of adsorbed intermediates. The ESM has recently been introduced to electrocatalysis by Exner and Over [20] and Chen et al. [21]. The ESM is general, and the only apparent assumption is that all elementary steps have the same pre-exponential factor. On this point, He et al. recently dicussed that the importance of the pre-exponential factor has been underestimated in electrochemistry [34].

This work presents a new notation that standardizes and simplifies the expressions of adsorbate coverage and overall reaction rate of any serial reaction network with first-order kinetics under steady state conditions. The reciprocal of the overall reaction rate is decomposed into a series of resistive terms, among which the largest term is defined as the rate-determining term (RDT). The RDT is the ratio of a thermodynamic term composed of thermodynamic constants of many elementary steps to a single forward-reaction rate. Generic analytical expressions for the Tafel- and volcano slopes are derived from the RDT, which are, to the best of our knowledge, an original contribution to the field.

This paper is organized as follows. We start by presenting the general formalism of the RDT and then derive analytical expressions of Tafel- and volcano slopes. Then, the RDT-based analysis is conducted on two reactions: the oxygen evolution reaction (OER), and the carbon dioxide reduction reactions (CDR). Afterwards, the RDT concept is compared with the RDS and PDS concepts in terms of the Tafel slope and the volcano plot of activity, revealing the cases in which the analytical approach to electrocatalytic reactions must to go beyond the RDS and PDS concepts and resort to the general RDT concept.

2. Theory

2.1. Rate determining term

We consider a multi-electron electrocatalytic reaction,

$$R + ne \leftrightarrow P, \tag{1}$$

where n, positive for reduction reactions and negative for oxidation reactions, is the number of electrons transferred in the reaction, and R and P denote the reactant and product. Several reaction intermediates, denoted as I_i ($i = 1, 2.., N$) with coverages θ_i, are interrelated with each other, forming a complex reaction network. The reaction network consists of many possible reaction pathways. In this work, we consider the simplest possible reaction pathway with first-order kinetics, namely a serial one that involves not more than one adsorbed intermediate on the reactant or product side of each elementary step. If we were to relax this assumption, rate equations would become nonlinear with terms of the form $\theta_i\theta_j$, where θ_i and θ_j are coverages of two intermediates involved in some elementary steps, or even higher order terms.

As shown in Fig. 1 (a), the serial reaction pathway considered here is composed of elementary steps

$$\begin{aligned} &R + * + n_1 e \leftrightarrow I_1, \\ &I_1 + n_2 e \leftrightarrow I_2, \\ &\quad \cdots \\ &I_{i-1} + n_i e \leftrightarrow I_i, \\ &\quad \cdots \\ &I_N + n_{N+1} e \leftrightarrow P + *, \end{aligned} \tag{2}$$

[1] There are other assumptions such as the neglect of double layer effects and mass transport phenomena.

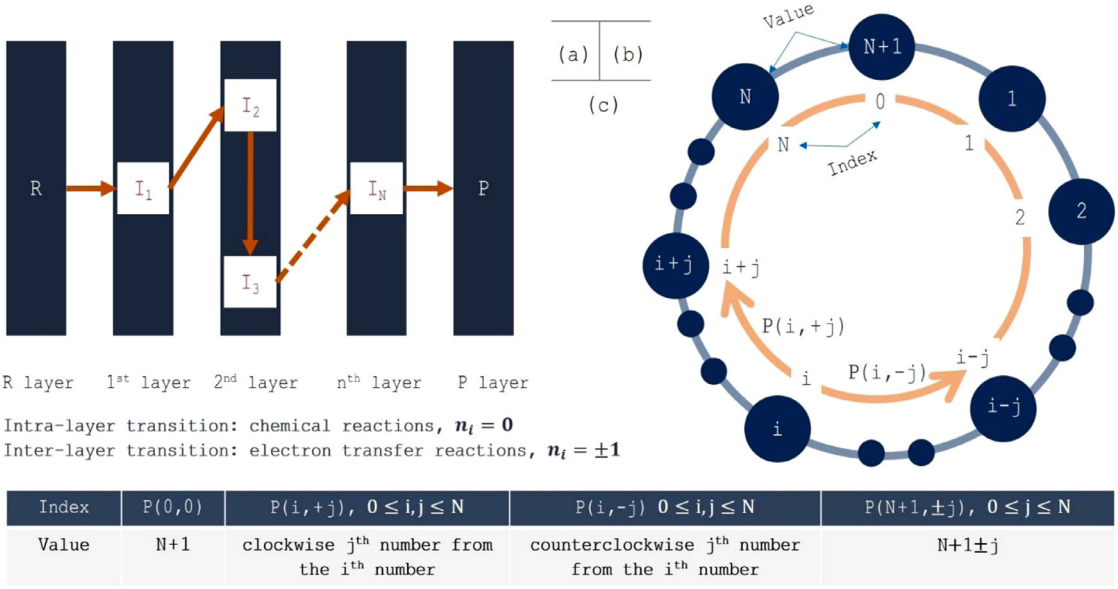

Index	P(0,0)	P(i,+j), $0 \le i,j \le N$	P(i,-j) $0 \le i,j \le N$	P(N+1,±j), $0 \le j \le N$
Value	N+1	clockwise j^{th} number from the i^{th} number	counterclockwise j^{th} number from the i^{th} number	N+1±j

Fig. 1. (a) A serial reaction network. (b) Schematic diagram of $P(i,\pm j)$. The outer circle corresponds to the value circle, and the inner circle corresponds to the index circle. (c) Calculation rules of $P(i,\pm j)$. $P(i,-j)$ points to the counterclockwise jth number from the ith number. $P(i,+j)$ points to the clockwise jth number from the ith number. In addition, we have, $P(0,\pm 0) = N+1$, and, $P(N+1,\pm j) = N+1\pm j,\ j = 0,1,2,..,N$.

where * denotes free sites for adsorption. Each elementary step may involve extra solution species, e.g., hydronium ions, which are not explicitly expressed in Eq. (2) but can be implicitly embedded into the rate constants, $k_i^{\pm}$ (+ forward reaction, - backward reaction).

The conservation of adsorption sites implies

$$\sum_{i=0}^{N} \theta_i = 1, \tag{3}$$

where θ_0 denotes the fraction of free sites for adsorption.

The conservation of electrons leads to

$$\sum_{i=1}^{N+1} n_i = n. \tag{4}$$

It is highly unlikely to transfer two or more electrons in an elementary step [35]. A rough estimate based on the Marcus theory indicates that the activation energy of a two-electron reaction will be four-fold of that for a single-electron reaction. Thus, n_i $(i = 1, 2.., N+1)$ is either zero or ± 1.

The net rates of elementary steps are written as

$$v_i = k_i^{+}\theta_{i-1} - k_i^{-}\theta_i,\ i = 1, 2.., N+1, \tag{5}$$

where $\theta_{N+1} = \theta_0$ closes the cycle. The rate constants, $k_i^{\pm}$, are calculated using the Butler-Volmer equation

$$k_i^{\pm} = k_i^0 \exp\left(-\frac{G_{a,i} \pm n_i\beta_i e(\phi_M - E_i)}{k_B T}\right), \tag{6}$$

where $G_{a,i}$ and E_i are the activation energy and equilibrium potential, k_i^0 the pre-exponential factor, ϕ_M the electrode potential, and β_i the symmetry factor of the ith step. Double layer effects, previously considered by Huang et al. [23], and Zhou et al. [19], are neglected here.

The change rates of intermediate coverages are given by

$$\frac{d\theta_i}{dt} = v_i - v_{i+1},\ i = 0, 1, 2 \ldots, (N-1). \tag{7}$$

Under steady state conditions, the N equations in Eq. (7) together with Eq. (3) form a closed set of equations, which after rearrangement can be written as

$$\begin{bmatrix} k_1^{+} & -k_1^{-} - k_2^{+} & k_2^{-} & \cdots & 0 \\ 0 & k_2^{+} & -k_2^{-} - k_3^{+} & \cdots & 0 \\ 0 & 0 & k_3^{+} & \cdots & 0 \\ \vdots & \vdots & \vdots & \vdots & \vdots \\ 1 & 1 & 1 & 1 & 1 \end{bmatrix} \begin{bmatrix} \theta_0 \\ \theta_1 \\ \theta_2 \\ \vdots \\ \theta_N \end{bmatrix} = \begin{bmatrix} 0 \\ 0 \\ 0 \\ \vdots \\ 1 \end{bmatrix}. \tag{8}$$

We can solve for θ_i from Eq. (8), which are expressed in an unified and compact form using a new formalism,

$$\theta_i = \frac{1}{\Xi}\sum_{j=0}^{N} \frac{\prod_{s=1}^{j} K_{\mathbf{P}(\mathbf{P}(i,-j),+s)}}{k^{-}_{\mathbf{P}(i,-j)}},\ i = 0, 1, 2, \ldots, N, \tag{9}$$

where the permutation operators $\mathbf{P}(i,\pm j)$, depicted in Fig. 1 (b) and illustrated in Fig. 1 (c), point to the jth number counted from the ith number in the counterclockwise (-) and clockwise (+) direction, respectively. $K_i = k_i^{+}/k_i^{-}$ is the equilibrium constant of the ith elementary step. The denominator of Eq. (9) Ξ normalizes θ_i, given by

$$\Xi = \sum_{i=0}^{N}\sum_{j=0}^{N} \frac{\prod_{s=1}^{j} K_{\mathbf{P}(\mathbf{P}(i,-j),+s)}}{k^{-}_{\mathbf{P}(i,-j)}} = \sum_{i=0}^{N} \frac{1}{k_{i+1}^{-}} \sum_{j=0}^{N}\prod_{s=1}^{j} K_{\mathbf{P}(i+1,+s)}. \tag{10}$$

The current density, defined as $j_{ss} = -ne\rho v_1$ (positive for oxidation, and negative for reduction), is calculated as

$$j_{ss} = -\frac{ne\rho}{\Xi}\left(\prod_{s=1}^{N+1} K_s - 1\right). \tag{11}$$

where ρ is the number density of active sites. $K_{\text{total}} = \prod_{s=1}^{N+1} K_s$ is the equilibrium constant of the total reaction, which is equal to 1 when the overall reaction is under equilibrium, namely, $j_{ss} = 0$. Eq. (11) is equivalent to the classical results obtained by Christiansen in 1953 for a serial reaction cycle [36]. Starting from Christiansen's formula and assuming the same pre-exponential factor for all the steps, Kozuch and Shaik represented the overall reaction rate in terms of energy quantities, and identified a rate-determining transition state and a rate-determining intermediate, which together give the energetic span [33]. With the aid of the graph-theoretic

method developed by King and Altman in 1956 [37], Kozuch extended the ESM for any reaction networks [38].

As $K_{\text{total}} \propto \exp(-nF\eta/RT)$, we have $K_{\text{total}} \gg 1$ when an overpotential η ($\eta < 0,\ n > 0$ for reduction and $\eta > 0, n < 0$ for oxidation) is applied. In the overpotential region of practical interest, it is safe to assume that $K_{\text{total}} \gg 1$. The inverse reaction rate (total reaction resistance) is given by

$$-\frac{ne\rho}{j_{ss}} \approx \sum_{i=1}^{N+1} \frac{\Theta_i}{k_i^+}, \tag{12}$$

where thermodynamic factors Θ_i are given by

$$\Theta_i = \frac{\sum_{j=0}^{N} \prod_{s=1}^{j} K_{\mathbf{P}(i,+s)}}{\prod_{s=1}^{N} K_{\mathbf{P}(i,+s)}}. \tag{13}$$

Eq. (12) decomposes the overall reaction resistance, $-\frac{ne\rho}{j_{ss}}$, into $(N+1)$ resistance terms. Each term has the same mathematical structure. Usually, one of the $(N+1)$ resistance terms is much larger than the rest because the reaction rates vary exponentially with the electrode potential, and determines the overall reaction resistance; this term is defined as the RDT. The RDT is the ratio of a thermodynamic term composed of thermodynamic constants of N elementary steps to a single forward-reaction rate. The uniformity of the mathematical structure of the resistance terms will remarkably reduce the complexity of kinetic analysis.

We take a step aside from the further formal analysis by considering a simple example to illustrate the formalism. The example involves only one intermediate and two electrons, thus, $N = 1$ and $n = 2$. The Volmer-Heyrovsky mechanism of the HER, $H^+ + e + * \leftrightarrow H_{ad}$, $H_{ad} + H^+ + e \leftrightarrow H_2 + *$, belongs to this category.

According to the algorithm shown in Fig. 1 (b), we have, $\mathbf{P}(0,-0) = \mathbf{P}(1,-1) = \mathbf{P}(\mathbf{P}(0,-1),+1) = 2$, $\mathbf{P}(0,-1) = \mathbf{P}(1,-0) = \mathbf{P}(\mathbf{P}(1,-1),+1) = 1$. Therefore, Ξ, expressed in Eq. (10), now reads

$$\begin{aligned}\Xi &= \frac{1}{k^-_{\mathbf{P}(0,-0)}} + \frac{K_{\mathbf{P}(\mathbf{P}(0,-1),+1)}}{k^-_{\mathbf{P}(0,-1)}} + \frac{1}{k^-_{\mathbf{P}(1,-0)}} + \frac{K_{\mathbf{P}(\mathbf{P}(1,-1),+1)}}{k^-_{\mathbf{P}(1,-1)}} \\ &= \frac{1}{k_2^-} + \frac{K_2}{k_1^-} + \frac{1}{k_1^-} + \frac{K_1}{k_2^-}.\end{aligned} \tag{14}$$

According to Eq. (9), θ_0 and θ_1 are written as

$$\begin{aligned}\theta_0 &= \frac{1}{\Xi}\left(\frac{1}{k^-_{\mathbf{P}(0,-0)}} + \frac{K_{\mathbf{P}(\mathbf{P}(0,-1),+1)}}{k^-_{\mathbf{P}(0,-1)}}\right) = \frac{1}{\Xi}\left(\frac{1}{k_2^-} + \frac{K_2}{k_1^-}\right) \\ &= \frac{k_1^- + k_2^+}{k_1^- + k_1^+ + k_2^- + k_2^+}, \\ \theta_1 &= \frac{1}{\Xi}\left(\frac{1}{k^-_{\mathbf{P}(1,-0)}} + \frac{K_{\mathbf{P}(\mathbf{P}(1,-1),+1)}}{k^-_{\mathbf{P}(1,-1)}}\right) = \frac{1}{\Xi}\left(\frac{1}{k_1^-} + \frac{K_1}{k_2^-}\right) \\ &= \frac{k_1^+ + k_2^-}{k_1^- + k_1^+ + k_2^- + k_2^+},\end{aligned} \tag{15}$$

which can be readily verified by solving Eq. (8) directly.

Afterwards, Eq. (12) becomes

$$-\frac{2e\rho}{j_{ss}} = \frac{\Theta_1}{k_1^+} + \frac{\Theta_2}{k_2^+}, \tag{16}$$

with thermodynamic factors given by

$$\begin{aligned}\Theta_1 &= \frac{1 + K_2}{K_2}, \\ \Theta_2 &= \frac{1 + K_1}{K_1}.\end{aligned} \tag{17}$$

The advantage of the presented formalism in kinetic analysis of electrocatalytic reactions becomes more apparent when N and n are larger, namely for more complex reactions, as in the case of oxygen evolution reaction and carbon dioxide reduction reaction considered at a later stage.

2.2. Tafel slope

The Tafel slope, b (mV dec^{-1}), is an important kinetic parameter in electrochemistry, which is widely used to infer mechanistic details of electrochemical reactions [30,31,35]. It is defined as

$$b = \mp \frac{dE}{d\ln(|j_{ss}|)}, \tag{18}$$

where E is the electrode potential; $-$ is for reduction reaction, and $+$ is for oxidation reaction. A related concept is the transfer coefficient, which, according to the IUPAC recommendation 2014 [35], can be calculated from b via

$$\alpha = \frac{k_B T}{be}. \tag{19}$$

If j_{ss} is approximated with the RDT, the task of calculating b of the total reaction is transformed to that of calculating α of the RDT, denoted, α_{RDT}. A closer examination on the RDT given in Eq. (12) reveals that α_{RDT} is given by

$$\alpha_{\text{RDT}} = \pm(\beta_i n_i + n_\Theta), \tag{20}$$

where β_i and n_i are the symmetry factor and the number of transferred electrons in the i^{th} step, corresponding to k_i^+ in the RDT, respectively. The positive sign (+) is for reduction reaction, and (-) for oxidation reaction. n_Θ is ascribed to Θ_i in the RDT, see Eq. (13). For the denominator of Θ_i, we have $\prod_{s=1}^{N} K_{\mathrm{P}(i,+s)} = K_{\text{total}}/K_i \propto \exp(-(n-n_i)F\eta/RT)$. There are $(N+1)$ terms in the numerator of Θ_i, $\sum_{j=0}^{N}\prod_{s=1}^{j} K_{\mathrm{P}(i,+s)}$, and, usually, one of them dominates over the rest and is generally written as $\prod_{s=1}^{j} K_{\mathrm{P}(i,+s)} \propto \exp(-\gamma F\eta/RT)$ with γ being the number of electrons involved in the dominating term in the numerator. Because only $(n-n_i)$ electrons are involved in the K terms in the numerator of Θ_i, we know that γ is within the range between 0 and $(n-n_i)$. Combined, n_Θ is obtained as

$$n_\Theta = (n - n_i) - \gamma, \tag{21}$$

where $(n-n_i)$ comes from the denominator of Θ_i, and γ from the numerator. Combining Eqs. (20) and (21), we see that α_{RDT} can have $(n-n_i+1)$ different values, ranging between $\pm\beta_i n_i$ and $\pm(n+(\beta_i-1)n_i)$, depending on which term dominates in the numerator of Θ_i.

2.3. Volcano plot of activity

We proceed to apply the RDT method to construct the volcano plot of activity. It has been well-documented that the binding energies of I_i ($i = 1, 2.., N$), denoted ΔG_i (a more negative ΔG_i means that the catalyst binds I_i more strongly), follow the scaling laws [7,13,39]

$$\Delta G_i = \Delta G_i^0 + f_i\left(\Delta G_j - \Delta G_j^0\right),\ i, j \in [1, N]. \tag{22}$$

Here, ΔG_i^0 and ΔG_j^0 are binding energies of ith and jth intermediates on a reference catalyst and f_i is a scaling coefficient. We have $f_0 = f_{N+1} = 0$ as Gibbs formation energies of the reactant and product are fixed and do not depend on ΔG_j. Eq. (22) implies that one of the binding energies can be used as the descriptor of the catalyst. Without loss of generality, we take ΔG_1 of I_1 as the descriptor. Neglecting further complications, such as lateral interac-

tions, as considered by Huang et al. [23], we calculate the equilibrium potential of the ith step as

$$E_i = -\frac{\Delta G_i - \Delta G_{i-1}}{n_i e} = E_i^0 - (f_i - f_{i-1})\frac{(\Delta G_1 - \Delta G_1^0)}{n_i e}, \tag{23}$$

with $E_i^0 = -(\Delta G_i^0 - \Delta G_{i-1}^0)/n_i e$. Note that Eq. (23) applies for electron transfer steps only, viz., $n_i \neq 0$.

At a fixed metal potential, ϕ_M, substituting Eq. (23) into Eq. (6) yields

$$k_i^+ \propto \exp\left(-\beta_i (f_i - f_{i-1})x\right) \tag{24}$$

where ϕ_M is embedded into a prefactor, which is unimportant here, and $x = (\Delta G_1 - \Delta G_1^0)/k_B T$ is the dimensionless descriptor. Accordingly, the equilibrium constant of the ith step depends on x as

$$K_i \propto \exp\left(-(f_i - f_{i-1})x\right). \tag{25}$$

Substituting k_i^+ with Eq. (24) and K_i with Eq. (25) in the RDT, we obtain a relationship between the overall reaction rate and the descriptor as

$$\ln|j_{ss}| \propto ((1-\beta_i)(f_i - f_{i-1}) + f_\forall)x, \tag{26}$$

where $f_\forall$ corresponds to the dominating term in the numerator of Θ_i, given by

$$f_\forall = \sum_{s=1}^{j} \left(f_{P(i,+s)} - f_{P(i,+s)-1}\right). \tag{27}$$

Eqs. (26) and (27) constitute a general formulation of the Volcano plot of activity.

3. Applications

The general formalism will be applied to two prototypical and technologically important reactions: the oxygen evolution reaction (OER) in alkaline media, which is the anodic reaction in water-splitting devices, and the carbon dioxide reduction (CDR) reaction in neutral media, which converts carbon dioxide to high-valued chemicals and fuels. The same analysis can be conducted for hydrogen evolution reaction and oxygen reduction reaction, such as in Refs. [23,40].

3.1. Oxygen evolution reaction (OER)

A general reaction pathway, as corroborated by first-principles studies, of the OER in alkaline media proceeds via [41–42]

$$OH^- + * \leftrightarrow OH_{ad} + e,$$

$$OH^- + OH_{ad} \leftrightarrow O_{ad} + H_2O + e,$$

$$OH^- + O_{ad} \leftrightarrow OOH_{ad} + e,$$

$$OH^- + OOH_{ad} \leftrightarrow O_2 + H_2O + * + e. \tag{28}$$

Here $*$ denotes the active sites, which are not needed to be specified in the present formulation. The OER involves three intermediates (OOH_{ad}, O_{ad}, OH_{ad}) and four electrons, thus, $N = 3$ and $n = -4$ (negative for oxidation reactions). For this case, the solution to Eq. (8) becomes very cumbersome. However, using the presented formalism expressed in Eq. (9), it is straightforward to obtain the expressions for θ_i as

$$\theta_0 = \frac{1}{\Xi}\left(\frac{1}{k_4^-} + \frac{K_4}{k_3^-} + \frac{K_3K_4}{k_2^-} + \frac{K_2K_3K_4}{k_1^-}\right),$$

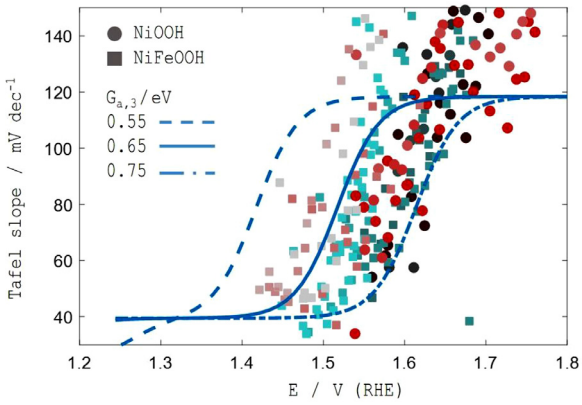

Fig. 2. Example of oxygen evolution reaction (OER). The theory and experiments are compared in terms of the Tafel slope. Experimental data were measured on NiOOH and NiFeOOH catalysts in 0.1M alkali MOH electrolytes (with M = Cs, K, Na and Li) from two research groups [43,44]. Sixteen experimental curves are included and there is no necessary to discern them herein. Parameters used in the calculation are $G_{a,1} = 0.63$ eV, $G_{a,2} = 0.70$ eV, $G_{a,3} = 0.55, 0.65, 0.75$ eV, $G_{a,4} = 0.65$ eV, $E_{eq,1} = 0.8$ V, $E_{eq,2} = 1.7$ V, $E_{eq,3} = 1.5$ V, $E_{eq,4} = 0.92$ V, $\beta_i = 0.5$, $n_i = 1$, $i = 1, 2, 3, 4$. Three theoretical curves correspond to different values of $G_{a,3}$.

$$\theta_1 = \frac{1}{\Xi}\left(\frac{1}{k_1^-} + \frac{K_1}{k_4^-} + \frac{K_1K_4}{k_3^-} + \frac{K_1K_4K_3}{k_2^-}\right),$$

$$\theta_2 = \frac{1}{\Xi}\left(\frac{1}{k_2^-} + \frac{K_2}{k_1^-} + \frac{K_2K_1}{k_4^-} + \frac{K_2K_1K_4}{k_3^-}\right),$$

$$\theta_3 = \frac{1}{\Xi}\left(\frac{1}{k_3^-} + \frac{K_3}{k_2^-} + \frac{K_3K_2}{k_1^-} + \frac{K_3K_2K_1}{k_4^-}\right), \tag{29}$$

with the number in the subscript indexing the elementary steps in Eq. (28). Using Eq. (10), we obtain Ξ as

$$\Xi = \frac{1 + K_1 + K_1K_2 + K_1K_2K_3}{k_4^-} + \frac{1 + K_4 + K_4K_1 + K_4K_1K_2}{k_3^-} + \frac{1 + K_3 + K_3K_4 + K_3K_4K_1}{k_2^-} + \frac{1 + K_2 + K_2K_3 + K_2K_3K_4}{k_1^-}. \tag{30}$$

The total reaction resistance is decomposed into

$$\frac{4e\rho}{j_{ss}} = \frac{\Theta_1}{k_1^+} + \frac{\Theta_2}{k_2^+} + \frac{\Theta_3}{k_3^+} + \frac{\Theta_4}{k_4^+}, \tag{31}$$

with thermodynamic factors

$$\Theta_1 = \frac{1 + K_2 + K_2K_3 + K_2K_3K_4}{K_2K_3K_4},$$

$$\Theta_2 = \frac{1 + K_3 + K_3K_4 + K_3K_4K_1}{K_1K_3K_4},$$

$$\Theta_3 = \frac{1 + K_4 + K_4K_1 + K_4K_1K_2}{K_1K_2K_4},$$

$$\Theta_4 = \frac{1 + K_1 + K_1K_2 + K_1K_2K_3}{K_1K_2K_3}. \tag{32}$$

In order to demonstrate that the present formulation possesses a wide range of applicability, we compare the theory with experimental data measured on NiOOH and NiFeOOH catalysts in 0.1M MOH electrolytes (with M = Cs, K, Na and Li) from two research groups [43,44]. Sixteen polarization curves are included in Fig. 2. The comparison beween the theory and experiments was conducted in terms of the Tafel slope. This way we circumvent the influence of several parameters that are difficult to determine in

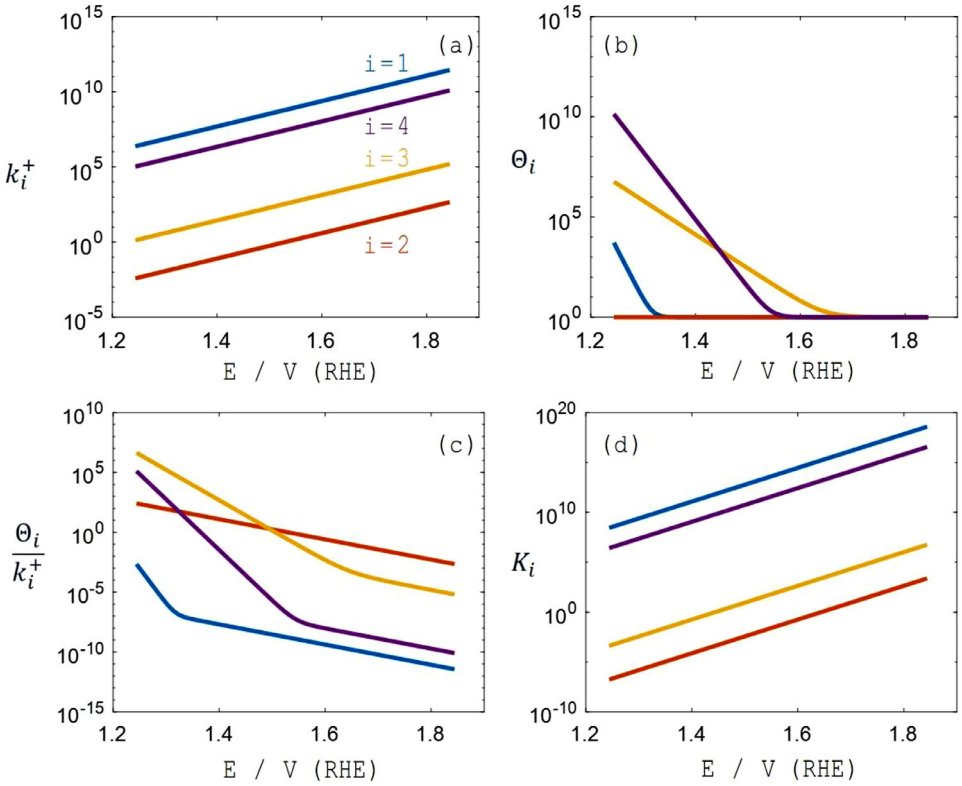

Fig. 3. (a) Four forward rate constants k_i^+, (b) four thermodynamic factors Θ_i, (c) four resistance terms $\frac{\Theta_i}{k_i^+}$, and (d) four K terms for the demonstration case of the oxygen evolution reaction with $G_{a,3} = 0.65$ eV.

experiments but may markedly change the polarization curve, including but not limited to the active surface area and the preexponential factors. All experimental curves more or less exhibit a single trend that the Tafel slope increases with the overpotential. Note in passing that the potential dependence of the Tafel slope throws doubt upon the routine practice of inferring the reaction mechanism from a specific value of the Tafel slope.

The solid lines in Fig. 2 are calculated from the theory using $G_{a,1} = 0.63$ eV, $G_{a,2} = 0.70$ eV, $G_{a,3} = 0.55/0.65/0.75$ eV, $G_{a,4} = 0.65$ eV, $E_{eq,1} = 0.8$ V, $E_{eq,2} = 1.7$ V, $E_{eq,3} = 1.5$ V, $E_{eq,4} = 0.92$ V, $\beta_i = 0.5$, $n_i = 1$, $i = 1, 2, 3, 4$. The theoretical curves show a slope in the intermediate voltage range, which agrees with the general trend of the experimental data. In addition, plateaus of 40 mV dec^{-1} and 120 mV dec^{-1} are seen at low and high overpotentials, respectively. By altering $G_{a,3}$ within ± 0.1 eV, the theoretical curves are able to envelop the experimental dots from the left to the right. We note that the Tafel slope cannot exceed 120 mV dec^{-1} when we assume $\beta_i = 0.5$ as usual. Tafel slopes larger than 120 mV dec^{-1} can be ascribed to several causes, including surface charging [23,45] (also known as Frumkin effects) and mass transport in solution [46,47].

Fig. 3 gives more details for the case of $G_{a,3} = 0.65$ eV. Fig. 3 (a) shows that the forward reaction rates k_i^+ increase exponentially with the electrode potential. Fig. 3 (b) shows the potential dependence of the thermodynamic factors Θ_i for the four elementary steps. All of the Θ_i's approach unity as the electrode potential increases, because $K_i \gg 1$ and the three-K_i product term dominates in the numerator.

Fig. 3 (c) reveals that the four resistances vary greatly, by orders of magnitude, from each other, justifying the assumption made previously that one of them dominates the total resistance at a given electrode potential or overpotential. Furthermore, the RDT transitions from $\frac{\Theta_3}{k_3^+}$ to $\frac{\Theta_2}{k_2^+}$ as the potential increases. In the low overpotential region (1.23 ~1.50 V_{RHE}), $\frac{\Theta_3}{k_3^+}$ is the RDT, and the dominating term in the numerator of Θ_3 is K_1K_4 because $K_1 \gg K_4 \gg 1 \gg K_2$, Fig. 3 (d). Therefore, $n_\Theta = -(n - n_i) + \gamma = (4 - 1) - 2 = 1$, $\alpha_{RDT} = 1.5$, and $b = 40$ mV dec^{-1}, corresponding to the plateau in the low overpotential range in Fig. 2. In the high overpotential region (above 1.50 V_{RHE}), $\frac{\Theta_2}{k_2^+}$ is the RDT, and the dominating term in the numerator of Θ_2 is $K_3K_4K_1$ because $K_1 \gg K_4 \gg K_3$, as shown in Fig. 3 (d). Therefore, $n_\Theta = -(n - n_i) + \gamma = (4 - 1) - 3 = 0$, $\alpha_{RDT} = 0.5$, and $b = 120$ mV dec^{-1}, which is again in accord with the high plateau in Fig. 2. In the intermediate overpotential range, the Tafel slope increases from 40 mV dec^{-1} to 120 mV dec^{-1}. We underline that a different set of model parameters may shift the Tafel slope curve along the electrode potential axis and change some detailed features, but the above analysis is generally valid.

In addition to the recent experimental data shown in Fig. 2, more experimental data of the Tafel slope of the OER on metal oxides have been collected by Doyle et al. [48]. The general trend, irrespective of specified properties of the catalyst, is the same as in Fig. 2, namely b increases as the overpotential increases, and levels off at 120 mV dec^{-1} in the limit of high overpotential. The basic principle behind the increasing trend of the Tafel slope is simply that K_i increases exponentially with the electrode potential (namely the overpotential), resulting in $K_i \gg 1$, and enventually, $\gamma = -3$, $n_\Theta = 0$, and $\alpha_{RDT} = 0.5$.

We proceed to apply the RDT method to construct the volcano plot of activity for the demonstration case of the OER. As summarized by Rossmeisl et al. [41,42,49], DFT calculations reveal that $\Delta G_{OOH} = \Delta G_{OH} + 3.2$ eV, $\Delta G_O = 2\Delta G_{OH} + 1.5$ eV, $\Delta G_{O_2} = 4.92$ eV. Therefore, we have, $f_1 = f_3 = 1$, $f_2 = 2$, $f_0 = f_4 = 0$. Fig. 4 (a) shows the volcano plot of the OER at 1.5 V_{SHE} with $\Delta G^0_{OH} = 0.6$ eV, and $G_{a,1} = 0.45$ eV, $G_{a,2} = 0.85$ eV, $G_{a,3} = 0.65$ eV, $G_{a,4} =$

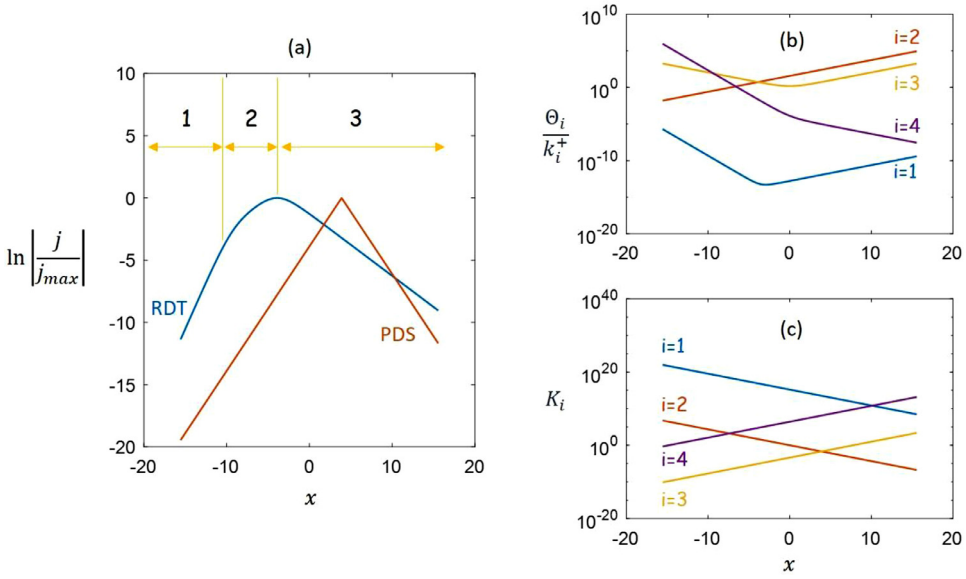

Fig. 4. (a) Volcano plot of OER at 1.5 V_{SHE}, (b) four resistance terms, (c) four K terms, calculated using $\Delta G^0_{OH} = 0.6$ eV, and $G_{a,1} = 0.45$ eV, $G_{a,2} = 0.85$ eV, $G_{a,3} = 0.65$ eV, $G_{a,4} = 0.50$ eV.

0.50 eV (a new set of activation energies are used here to enlarge the regime 2). As the descriptor x, defined as $x = (\Delta G_{OH} - \Delta G^0_{OH})/k_BT$, increases from −15 to 15, $\lg(|j_{ss}|)$ increases first rapidly (regime 1), then gradually (regime 2), and finally decreases (regime 3). In regime 1, Θ_4/k_4 is the RDT, Fig. 4 (b), and the dominating term in the numerator of Θ_4 is K_1K_2, Fig. 4 (c). Therefore, Eq. (27) indicates that $f_\forall = f_1 - f_0 + f_2 - f_1 = 2$, then Eq. (26) yields $\ln|j_{RDT}| \propto ((1-\beta_4)(f_4 - f_3) + f_\forall)x = 1.5x$. In regime 2, Θ_3/k_3 is the RDT, and the dominating term in the numerator of Θ_3 is $K_4K_1K_2$. Therefore, we have $f_\forall = f_4 - f_3 + f_1 - f_0 + f_2 - f_1 = 1$, and $\ln|j_{RDT}| \propto ((1-\beta_3)(f_3 - f_2) + f_\forall)x = 0.5x$. In comparison, the slope of the curve in regime 2 is 0.5, while that in regime 1 is 1.5. In regime 3, Θ_2/k_2 is the RDT, and the dominating term in the numerator of Θ_2 is $K_3K_4K_1$. Therefore, we have $f_\forall = f_3 - f_2 + f_4 - f_3 + f_1 - f_0 = -1$, and $\ln|j_{RDT}| \propto ((1-\beta_2)(f_2 - f_1) + f_\forall)x = -0.5x$, indicating a decreasing trend. The comparison of the volcano plot with that calculated from the PDS concept is deferred to the discussion section.

3.2. Carbon dioxide reduction (CDR)

We proceed to apply the RDT concept to the reduction of CO_2 to CO, which occurs via the following elementary steps [50–52],

$$CO_2 + H_2O + * + e \leftrightarrow COOH_{ad} + OH^-,$$

$$COOH_{ad} + H_2O + e \leftrightarrow CO_{ad} + OH^-,$$

$$CO_{ad} \leftrightarrow CO(aq) + *, \tag{33}$$

The CDR involves two intermediates ($COOH_{ad}$ and CO_{ad}) and transfers two electrons, thus, $N = 2$ and $n = 2$. Using the presented formalism expressed in Eq. (9), the expressions for θ_i are written as,

$$\theta_0 = \frac{1}{\Xi}\left(\frac{1}{k_3^-} + \frac{K_3}{k_2^-} + \frac{K_2K_3}{k_1^-}\right),$$

$$\theta_1 = \frac{1}{\Xi}\left(\frac{1}{k_1^-} + \frac{K_1}{k_3^-} + \frac{K_1K_3}{k_2^-}\right),$$

$$\theta_2 = \frac{1}{\Xi}\left(\frac{1}{k_2^-} + \frac{K_2}{k_1^-} + \frac{K_1K_2}{k_3^-}\right), \tag{34}$$

with the number in the subscript indexing the elementary steps in Eq. (33). Using Eq. (10), we obtain Ξ as

$$\Xi = \frac{1 + K_1 + K_1K_2}{k_3^-} + \frac{1 + K_3 + K_3K_1}{k_2^-} + \frac{1 + K_2 + K_2K_3}{k_1^-}. \tag{35}$$

The total reaction resistance is decomposed into

$$-\frac{2e\rho}{j_{ss}} = \frac{\Theta_1}{k_1^+} + \frac{\Theta_2}{k_2^+} + \frac{\Theta_3}{k_3^+}, \tag{36}$$

with thermodynamic factors

$$\Theta_1 = \frac{1 + K_2 + K_2K_3}{K_2K_3},$$

$$\Theta_2 = \frac{1 + K_3 + K_3K_1}{K_1K_3},$$

$$\Theta_3 = \frac{1 + K_1 + K_1K_2}{K_1K_2}, \tag{37}$$

Fig. 5(a) exhibits the theory-experiment comparison in terms of the Tafel slope as a function of the electrode potential. The experimental data were obtainded by differentiating the polarization curves taken from Ref. [53] which were measured at Ag electrodes with different crystral structures. The leftmost solid line in Fig. 5(a) is calculated using the present theory with $G_{a,1} = 0.54$ eV, $G_{a,2} = 1.2$ eV, $G_{a,3} = 0.35$ eV, $G_{a,-3} = 0.75$ eV, $E_{eq,1} = -0.9$ V, $E_{eq,2} = 0.4$ V, $\beta_i = 0.5$, $n_i = 1$, $i = 1, 2$. The activation barriers are taken from Ref. [54]. The equilibrium potentials are calculated based on binding energies in Ref. [55]. The solution conditions are pH = 7, $c_{CO_2} = 0.034$M, corresponding to the 0.1M $KHCO_3$ solution saturated with CO_2 of a partial pressure 101 kPa. c_{CO} is assumed to be 0.001 M considering the quick escape of generated CO. The theoretical curve captures the general trend that the Tafel slope increases with the overpotential, as observed in experimental data. Theoretical curves with $G_{a,2} = 1.2$ and 1.0 eV envelop the experimental dots. Same results can be obtained by increasing $G_{a,1}$ from 0.54 to 0.74 eV while keeping $G_{a,2} = 1.2$ eV. The origin of these variations will be explained in

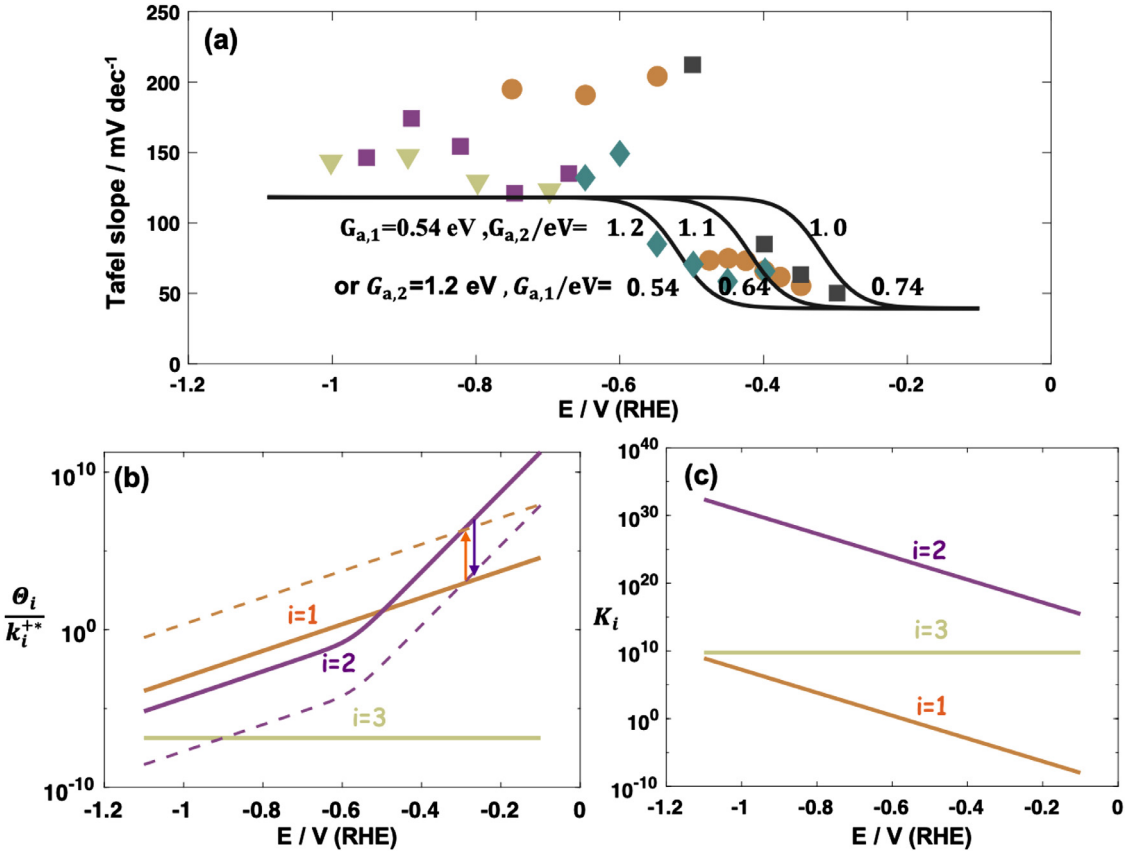

Fig. 5. Example of carbon dioxide reduction (CDR): (a) comparison between the theory and experiments in terms of the Tafel slope. experimental data were measured at Ag catalysts with different structures [53]. Parameters used in the calculation are given in the main text. (b) Three resistance terms, (c) Three K terms.

the next paragraph. In addition, altering $E_{eq,1}$ or $E_{eq,2}$ within 0.4 V while keeping $G_{a,1}$ and $G_{a,2}$ constant has the same effect, because $k_i \propto \exp(-\frac{G_{a,i}\pm n_i\beta_i e(\phi_M - E_{eq,i})}{k_B T})$ and $\beta_1 = \beta_2 = 0.5$. Independent information of these parameters, which could be obtained from DFT calculations, will be needed to remove this ambiguity.

For the case of $G_{a,2} = 1.2$eV and $G_{a,1} = 0.54$ eV, the RDT transitions from $\frac{\Theta_2}{k_2^+}$ to $\frac{\Theta_1}{k_1^+}$ as the overpotential increases, as shown in Fig. 5(b) (the solid lines). In the low overpotential region (-0.1 ~-0.5 V_{RHE}), $\frac{\Theta_2}{k_2^+}$ is the RDT, and the dominating term in the numerator of Θ_2 is K_3 because $K_3 \gg 1 \gg K_1$, Fig. 5(c). Therefore, $n_\Theta = (n - n_i) - \gamma = (2-1) - 0 = 1$, $\alpha_{RDT} = 1.5$, and $b = 40$ mV dec^{-1}, corresponding to the plateau in the low overpotential range in Fig. 5(a). In the high overpotential region (below -0.60 V_{RHE}), $\frac{\Theta_1}{k_1^+}$ is the RDT, and the dominating term in the numerator of Θ_1 is K_2K_3 because $K_2 \gg K_3 \gg 1$, as shown in Fig. 5(c). Therefore, $n_\Theta = (n - n_i) - \gamma = (2-1) - 1 = 0$, $\alpha_{RDT} = 0.5$, and $b = 120$ mV dec^{-1}, in accord with the high plateau in Fig. 5(a). In the intermediate overpotential range, the Tafel slope increases from 40 mV dec^{-1} to 120 mV dec^{-1}. Again, Tafel slopes higher than 120 mV dec^{-1} could be caused by surface charging and mass transport effects, which are not considered in this theory. With decreasing $G_{a,2}$, $\frac{\Theta_2}{k_2^+}$ decreases for k_2^+ increases, see the purple dashed line in Fig. 5(b). As a result, the transition potential is shifted to a more positive value, so is the Tafel slope curve. With increasing $G_{a,1}$, $\frac{\Theta_1}{k_1^+}$ is shifted up, see the yellow dashed line. In this case, the transition potential is shifted to a more positive value, too. Consequently, the same Tafel slope is obtained.

The RDT concept is then used to construct the volcano plot of activity for the CDR. Fig. 6(a) shows the volcano plot of the CDR at -0.8 V_{RHE} using ΔG_{CO} as the descriptor. The scaling relation used here is $\Delta G_{COOH} = 0.7 * \Delta G_{CO} + 0.7$ eV, which was obtained at 211 facets of an array of transition metals [51]. Thus, $f_1 = 0.7$, $f_2 = 1$, $f_0 = f_3 = 0$. As the descriptor x, defined as $x = (\Delta G_{CO} - \Delta G_{CO}^0)/k_BT$, increases from -24 to 24, $\lg(|j_{ss}|)$ first increases rapidly in regime 1, then decreases gradually in regime 2. In regime 1, Θ_3/k_3 is the RDT, Fig. 6(b), and the dominating term in the numerator of Θ_3 is K_1K_2, Fig. 6(c). Therefore, Eq. (27) indicates that $f_\forall = f_1 - f_0 + f_2 - f_1 = 1$, and Eq. (26) yields $\ln|j_{RDT}| \propto f_\forall x = 1x$. In regime 2, Θ_1/k_1 is the RDT, and the dominating term in the numerator of Θ_1 is K_2K_3. Therefore, we have $f_\forall = f_2 - f_1 + f_3 - f_2 = -0.7$, and $\ln|j_{RDT}| \propto ((1-\beta_1)(f_1 - f_0) + f_\forall)x = -0.35x$, indicating a decreasing trend in the volcano plot of activity.

4. Discussion

4.1. Comparison of the RDT with the RDS concept

The RDS concept assumes that there exists a slow step that controls the rate of the overall reaction whereas other steps are in quasi-equilibrium, and that the reaction surface is nearly void of adsorbed intermediates. A corollary of the first assumption is that, for reduction reactions, the forward reaction rate of the RDS is much higher than the backward one. Consequently, the rate of the overall reaction is given by

$$\frac{-j_{RDS}}{ne\rho k^0_{N_{RDS}}} = \left[I_{N_{RDS}-1}\right] \exp\left(-\frac{G_{a,N_{RDS}} + n_{N_{RDS}}\beta_{N_{RDS}} e\left(\phi_M - E_{N_{RDS}}\right)}{k_B T}\right), \quad (38)$$

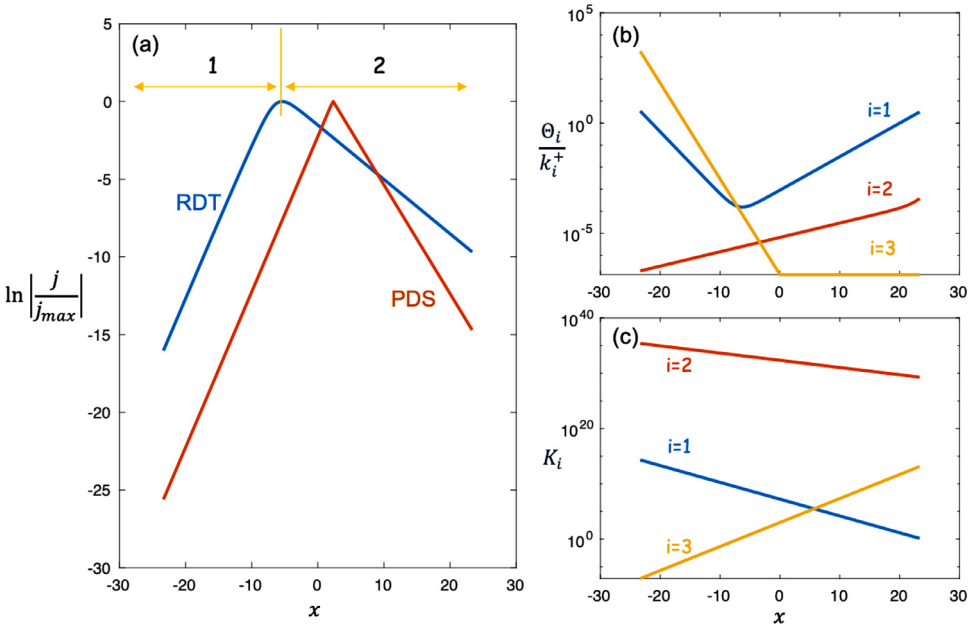

Fig. 6. (a) Volcano plot of CDR at -0.8 V_{RHE}, (b) three resistance terms, (c) three K terms, calculated using $\Delta G^0_{CO} = 0.0$ eV,$G_{a,1} = 0.54$ eV, $G_{a,2} = 1.2$ eV, $G_{a,3} = \max(0.35, 0.35 - \Delta G_{CO})$ eV, $G_{a,-3} = \max(0.35, 0.35 + \Delta G_{CO})$ eV, with 0.35 eV being the minimum activation energy of Step 3 (the solvent reorganization energy) [54], and solution conditions, pH = 7, $c_{CO_2} = 0.034$M, $c_{CO} = 0.001$M.

where N_{RDS} is the location of the RDS in the reaction sequence, $[I_{N_{RDS}-1}]$ denotes the normalized concentration of $I_{N_{RDS}-1}$, viz., the reactant in the RDS. As the $(N_{RDS} - 1)$ steps prior to the RDS are in quasi-equilibrium, $[I_{N_{RDS}-1}]$ is derived from [R], the normalized concentration of the reactant, taken to be unity, via

$$[I_{N_{RDS}-1}] = \prod_{s=1}^{N_{RDS}-1} K_s = \exp\left(-\sum_{s=1}^{N_{RDS}-1} \frac{n_s e(\phi_M - E_s)}{k_B T}\right). \quad (39)$$

The apparent transfer coefficient is then calculated as

$$\alpha_{RDS} = \pm\left(\beta_i n_i + \sum_{s=1}^{N_{RDS}-1} n_s\right). \quad (40)$$

Compared with α_{RDT} in Eqs. (20) and (21) which is based on the RDT concept, α_{RDS} in Eq. (40) involves N_{RDS} as a parameter, implying that the position of the RDS in the sequence is possible to be inferred from α_{RDS}. For example, a Tafel slope of 120 mV dec^{-1} has been taken as the indicator of the Volmer step as the RDS in the HER [30]. On the contrary, this position information is completely lost in α_{RDT}. The underlying cause of this difference is that the conservation of adsorption sites expressed in Eq. (3) couples all steps. This coupling is discarded in the RDS concept due to the second assumption that the electrode surface is nearly void of adsorbates. If we take the RDS as the "present", steps prior to the RDS as the "past", and those behind the RDS as the "future", Eq. (3) couples the "past", the "present" and the "future", excluding the possibility of identifying the time, namely, the location of the RDS.

As regards the dependence of catalytic activity on the binding energies of reaction intermediates, substituting Eqs. (24) and (25) into Eqs. (38) and (39) yields

$$\ln|j_{RDS}| \propto -\left(\beta_{N_{RDS}} f_{N_{RDS}} + \left(1 - \beta_{N_{RDS}}\right) f_{N_{RDS}-1}\right)x. \quad (41)$$

In the example of the OER, f_i is nonnegative, implying that $\ln|j_{qe}|$ decreases monotonically with x. It then comes as a surprise that the volcano plot of activity disappears in kinetic analyses based on the RDS concept. The problem lies in the second assumption that the reaction surface is nearly void of adsorbed intermediates, which implies that adsorption of reaction intermediates is weak. Consequently, the activity shall decrease, according to the Sabatier principle, if the binding energy shifts to more positive values, namely, the binding strength becomes weaker.

4.2. Comparison of the RDT with the PDS concept

The basic idea of PDS is explained in the context of the reaction mechanism expressed in Eq. (2). At given ϕ_M, the reaction Gibbs energies of elementary steps are calculated as

$$\Delta\Delta G_i = \Delta G_i - \Delta G_{i-1} + n_i e\phi_M, \ i = 1, 2, \ldots, (N + 1). \quad (42)$$

The step with the most positive $\Delta\Delta G_i$ is termed the PDS, because it is the last step whose $\Delta\Delta G_i$ turns negative upon decreasing (increasing) ϕ_M for reduction (oxidation) reactions. The lowest overpotential that is sufficient to render all the $\Delta\Delta G_i$ negative is termed the thermodynamic overpotential. The catalytic activity is calculated as

$$-\frac{j_{PDS}}{ne\rho k^0_{PDS}} = \exp\left(-\frac{\Delta\Delta G_{PDS}}{k_B T}\right). \quad (43)$$

Combining Eqs. (42) and (43), it becomes clear that the PDS concept gives a constant Tafel slope depending on the transfer coefficient put in Eq. (43). Consequently, the PDS concept cannot generate potential-dependent Tafel slopes.

Substituting Eq. (22) into Eq. (42) yields

$$\Delta\Delta G_i = (f_i - f_{i-1})\left(\Delta G_1 - \Delta G^0_1\right) + n_i e\left(\phi_M - E^0_i\right). \quad (44)$$

When $(\Delta G_1 - \Delta G^0_1)$ is sufficiently negative, to offset the influence of $n_i e(\phi_M - E^0_i)$, the PDS is the step with the most negative $(f_i - f_{i-1})$, and $|j_{PDS}|$ increases as $(\Delta G_1 - \Delta G^0_1)$ shifts positively, resulting in an ascending branch of the volcano plot. The PDS transitions to the step with the most positive $(f_i - f_{i-1})$ when $(\Delta G_1 - \Delta G^0_1)$ is sufficiently positive, and $|j_{PDS}|$ decreases as $(\Delta G_1 - \Delta G^0_1)$ shifts positively, resulting in a descending branch of the volcano plot.

As regards the OER example, the PDS-derived volcano plot is shown in Fig. 4 (a), which is symmetrical. As $(f_3 - f_2) = (f_4 - f_3) = -1$, thus assuming the most negative value of $(f_i - f_{i-1})$, the third or fourth step can be the PDS on the ascending branch. A more detailed comparison shows $\Delta\Delta G_3 = 1.1$ eV –

$(\Delta G_1 - \Delta G_1^0)$ and $\Delta\Delta G_4 = 0.4\ \text{eV} - (\Delta G_1 - \Delta G_1^0)$, indicating that the third step, whose reaction free energy is more positive, is the PDS on the ascending branch. The same line of reasoning suggests that $\Delta\Delta G_2 = 0.9\ \text{eV} + (\Delta G_1 - \Delta G_1^0)$ is the PDS on the descending branch. The volcano apex is obtained at $\Delta\Delta G_3 = \Delta\Delta G_2$, namely, $(\Delta G_1 - \Delta G_1^0) = 0.1$ eV and $x = 3.9$.

The PDS-derived volcano plot for the CDR is shown in Fig. 6(a). As $(f_1 - f_0) = 0.7$, $(f_2 - f_1) = 0.3$, the first step with most positive value of $(f_i - f_{i-1})$, is the PDS on the descending branch, and the slope is -0.7. $(f_3 - f_2) = -1$ is the only negative value among $(f_i - f_{i-1})$, thus the third step is the PDS on the ascending branch, with slope 1. The volcano apex is obtained at $\Delta\Delta G_3 = \Delta\Delta G_1$, namely, $x = 2.3$, as seen in Fig. 6(a).

4.3. When to use the RDT

In this section, we address the questions when the RDT is equivalent to the RDS or the PDS, and when the RDS and PDS are no longer sufficient and the RDT shall be used.

The RDT-based analysis is divided into three steps. First, we need to postulate the reaction mechanism, as in Eq. (2). Second, we have to solve the closed set of rate equations, as in Eq. (8), and obtain an analytical expression for the total reaction rate. Third, we must identify the RDT in the total reaction rate.

The first step in the above three-step procedure is also involved in the RDS method. By assuming that the electrode surface is nearly void of adsorbed intermediates and that there exists a step with slowest kinetics, the RDS method greatly simplifies the second step, and the total reaction rate of any electrochemical reaction can be in principle obtained via a simple route. The RDS method, which is essentially a simplified version of the RDT method, gives the same results as the RDT method when both assumptions are fulfilled. However, the electrode surface used for electrocatalytic reactions is usually covered, to a considerable extent, by reaction intermediates, defying the basic assumption of the RDS method. That is the reason why the RDS method brings about a monotonically decreasing relation between activity and binding strength, and fails to yield the volcano plot. Nevertheless, the RDS method is applicable to outer-sphere electrochemical reactions where reaction intermediates do not adsorb onto the electrode surface.

In sharp contradiction with the RDS and RDT methods, the PDS concept is entirely based on thermodynamic reasoning, while kinetics is not considered. Neglect of kinetics reduces the mathematic complexity and generalizes its applicability. However, this drastic simplification introduces some caveats and even errors. For instance, the PDS concept results in a constant Tafel slope, independent of the electrode potential. Furthermore, as shown in Fig. 3(a), the volcano apex is located on the negative half axis for the RDT-derived volcano plot, but on the positive half axis for the PDS-derived one. The PDS concept is valid when the difference in the activation barriers is much smaller than that in the reaction free energies for all elementary steps. Otherwise, the PDS concept leads to incorrect, even qualitatively, conclusions. A recent example for the inadequacy of this concept is the activity sequence of Pt(111), Ir(111), and Rh(111) for the ORR [19]. These three metals belong to the strongly adsorbing branch of the volcano plot of the ORR. Single crystal experiments unravel the binding strength order Pt(111) < Ir(111) < Rh(111) for hydroxyl, an reaction intermediate of ORR. Therefore, we expect an activity sequence Pt(111) > Ir(111) > Rh(111) according to the PDS concept. However, experimental data show an activity trend Pt(111) > Rh(111) > Ir(111) for ORR. The discrepancy was attributed to kinetic factors, namely, a much higher activation energy at Ir(111) than Rh(111), which however violates the Brønsted–Evans–Polanyi relationship.

5. Conclusions

This work presented a new formalism and analytical concept for the steady-state kinetics of electrocatalytic reactions with first-order kinetics. The determining term in the overall reaction rate was defined in general mathematical form. From the rate-determining term (RDT), we derived analytical expressions for the Tafel slope and slopes in the volcano plot of activity. A comparison with the rate-determining step (RDS) and potential-determining step (PDS) concepts revealed crucial assumptions restricting the viability and utility of the latter two concepts in electrocatalysis.

For electrocatalytic reactions, the RDS gives erroneous results in most cases except when the coverages of adsorbed intermediates are negligible. Specifically, the practice of identifying the RDS in a multistep reaction mechanism using the measured Tafel slope is questionable in general. The RDS method always gives a decreasing relation between the activity and the binding strength, and is unable to yield a volcano plot of activity.

The PDS is a straightforward and general concept that is able to yield the correct activity trend and thus guide the search for more active catalysts, when all complications due to multistep kinetics can be neglected. Therefore, the PDS concept is unable to explain important kinetic phenomena, such as potential-dependent Tafel slopes. The RDT concept, by providing a generalized treatment that explicitly treats the multistep kinetics, is expected to improve over the PDS concept, though additional cost must be paid to determine the activation barriers of elementary steps, which is a task for computation and experimentation. Care must be exercised when employing the PDS concept to predict the activity sequence of a specific set of catalysts, especially, when the activation energies vary greatly inbetween.

Before closing the paper, we add a few remarks on the limitations of the RDT method presented herein. The foremost limitation is the use of a serial reaction network with first-order kinetics. In many cases, the reaction network exhibits a more complicated coupling, leading to nonlinear terms in the kinetic rate equations. In such cases, analytical solution is usually impossible without additional assumptions. For example, in order to drop the nonlinear term, Huang et al. assumed the coverage of OOH_{ad} to be zero in the microkinetic modelling of ORR [23]. Furthermore, lateral interaction between adsorbates, surface charging effects and mass transport phenomena are not considered in this work. Treatment of these factors in electrocatalysis can be found in the literature [19,23,40,56]. Last, the kinetic rates are calculated using the Butler-Volmer equation with a transfer coefficient of 0.5. It is known that the Butler-Volmer equation overestimates the kinetic rate in high-overpotential region where the Marcus-Hush-Chidsey theory gives more accurate results [57,58]. In addition, the transfer coefficient of 0.5 is a first approximation, as discussed in Ref. [8]. Recently, Zhang and Huang employed the Marcus-Hush-Chidsey theory to describe the Peroxodisulfate Reduction at Pt(111), asserting that the Marcus-Hush-Chidsey theory is essential for explaining the anomalous current decay at high overpotentials [56].

Declaration of Competing Interest

The author declares that they have no known competing financial interests or personal relationships that could have appeared to influence the work reported in this paper.

Credit authorship contribution statement

Jun Huang: Conceptualization, Data curation, Formal analysis, Funding acquisition, Visualization, Writing – original draft, Writing – review & editing. **Xinwei Zhu:** Data curation, Formal analysis, Visualization, Writing – original draft, Writing – review & editing. **Michael Eikerling:** Conceptualization, Funding acquisition, Supervision, Project administration, Writing – review & editing.

Acknowledgment

J.H. acknowledges the funding provided by the Alexander von Humboldt Foundation. ME acknowledges the financial support from Forschungszentrum Juelich GmbH. Useful discussion with Axel Groß are gratefully acknowledged.

References

[1] S. Chu, Y. Cui, N. Liu, The path towards sustainable energy, Nat. Mater. 16 (2017) 16–22.
[2] V.R. Stamenkovic, D. Strmcnik, P.P. Lopes, N.M. Markovic, Energy and fuels from electrochemical interfaces, Nat. Mater. 16 (2017) 57–69.
[3] B. Hammer, J.K. Norskov, Why gold is the noblest of all the metals, Nature 376 (1995) 238–240.
[4] N.M. Marković, P.N. Ross, Surface science studies of model fuel cell electrocatalysts, Surf. Sci. Rep. 45 (2002) 117–229.
[5] E. Santos, P. Quaino, W. Schmickler, Theory of electrocatalysis: hydrogen evolution and more, Phys. Chem. Chem. Phys. 14 (2012) 11224–11233.
[6] W. Schmickler, K. Uosaki, On the theory of electrocatalysis, in: Electrochemical Science for a Sustainable Society: A Tribute to John O'M Bockris, Springer International Publishing, Cham, 2017, pp. 95–111.
[7] J.K. Nørskov, T. Bligaard, B. Hvolbæk, F. Abild-Pedersen, I. Chorkendorff, C.H. Christensen, The nature of the active site in heterogeneous metal catalysis, Chem. Soc. Rev. 37 (2008) 2163–2171.
[8] H. Ooka, J. Huang, K.S. Exner, The sabatier principle in electrocatalysis: basics, limitations, and extensions, 9 (2021).
[9] K.J. Laidler, A glossary of terms used in chemical kinetics, including reaction dynamics (IUPAC Recommendations 1996), Pure Appl. Chem. 68 (1996) 149–192.
[10] S. Kozuch, J.M.L. Martin, The rate-determining step is dead. long live the rate-determining state!, ChemPhysChem 12 (2011) 1413–1418.
[11] J.K. Nørskov, J. Rossmeisl, A. Logadottir, L. Lindqvist, J.R. Kitchin, T. Bligaard, H. Jónsson, Origin of the overpotential for oxygen reduction at a fuel-cell cathode, J. Phys. Chem. B 108 (2004) 17886–17892.
[12] E. Santos, W. Schmickler, d-Band catalysis in electrochemistry, ChemPhysChem 7 (2006) 2282–2285.
[13] J.K. Nørskov, T. Bligaard, J. Rossmeisl, C.H. Christensen, Towards the computational design of solid catalysts, Nat. Chem. 1 (2009) 37–46.
[14] M.T.M. Koper, Analysis of electrocatalytic reaction schemes: distinction between rate-determining and potential-determining steps, J. Solid State Electrochem. 17 (2013) 339–344.
[15] W. Chen, J. Huang, J. Wei, D. Zhou, J. Cai, Z.D. He, Y.X. Chen, Origins of high onset overpotential of oxygen reduction reaction at Pt-based electrocatalysts: a mini review, Electrochem. Commun. 96 (2018) 71–76.
[16] I.E.L. Stephens, A.S. Bondarenko, U. Grønbjerg, J. Rossmeisl, I. Chorkendorff, Understanding the electrocatalysis of oxygen reduction on platinum and its alloys, Energy Environ. Sci. 5 (2012) 6744–6762.
[17] A. Kulkarni, S. Siahrostami, A. Patel, J.K. Nørskov, Understanding catalytic activity trends in the oxygen reduction reaction, Chem. Rev. 118 (2018) 2302–2312.
[18] A.M. Gómez-Marín, R. Rizo, J.M. Feliu, Oxygen reduction reaction at Pt single crystals: a critical overview, Catal. Sci. Technol. 4 (2014) 1685–1698.
[19] D. Zhou, J. Wei, Z.D. He, M.L. Xu, Y.X. Chen, J. Huang, Combining single crystal experiments and microkinetic modeling in disentangling thermodynamic, kinetic, and double-layer factors influencing oxygen reduction, J. Phys. Chem. C 124 (2020) 13672–13678.
[20] K.S. Exner, H. Over, Kinetics of electrocatalytic reactions from first-principles: a critical comparison with the Ab initio thermodynamics approach, Acc. Chem. Res. 50 (2017) 1240–1247.
[21] J. Chen, Y. Chen, P. Li, Z. Wen, S. Chen, Energetic span as a rate-determining term for electrocatalytic volcanos, ACS Catal. 8 (2018) 10590–10598.
[22] H.A. Hansen, V. Viswanathan, J.K. Nørskov, Unifying kinetic and thermodynamic analysis of 2 e– and 4 e– reduction of oxygen on metal surfaces, J. Phys. Chem. C 118 (2014) 6706–6718.
[23] J. Huang, J. Zhang, M. Eikerling, Unifying theoretical framework for deciphering the oxygen reduction reaction on platinum, Phys. Chem. Chem. Phys. 20 (2018) 11776–11786.
[24] K.S. Exner, Why the microkinetic modeling of experimental tafel plots requires knowledge of the reaction intermediate's binding energy, Electrochem. Sci. Adv. (2021) e2100037 n/a.
[25] J.O.M. Bockris, Z. Nagy, Symmetry factor and transfer coefficient. A source of confusion in electrode kinetics, J. Chem. Educ. 50 (1973) 839.
[26] C.T. Campbell, Finding the rate-determining step in a mechanism: comparing dedonder relations with the "degree of rate control", J. Catal. 204 (2001) 520–524.
[27] J.A. Dumesic, Reply to finding the rate-determining step in a mechanism: comparing dedonder relations with the "degree of rate control", J. Catal. 204 (2001) 525–529.
[28] J.A. Dumesic, Analyses of reaction schemes using de donder relations, J. Catal. 185 (1999) 496–505.
[29] C. Stegelmann, A. Andreasen, C.T. Campbell, Degree of rate control: how much the energies of intermediates and transition states control rates, J. Am. Chem. Soc. 131 (2009) 8077–8082.
[30] T. Shinagawa, A.T. Garcia-Esparza, K. Takanabe, Insight on Tafel slopes from a microkinetic analysis of aqueous electrocatalysis for energy conversion, Sci. Rep. 5 (2015) 13801.
[31] A.T. Marshall, L. Vaisson-Béthune, Avoid the quasi-equilibrium assumption when evaluating the electrocatalytic oxygen evolution reaction mechanism by Tafel slope analysis, Electrochem. Commun. 61 (2015) 23–26.
[32] M.K. Sabbe, M.F. Reyniers, K. Reuter, First-principles kinetic modeling in heterogeneous catalysis: an industrial perspective on best-practice, gaps and needs, Catal. Sci. Technol. 2 (2012) 2010–2024.
[33] S. Kozuch, S. Shaik, How to conceptualize catalytic cycles? The energetic span model, Acc. Chem. Res. 44 (2011) 101–110.
[34] Z.D. He, Y.X. Chen, E. Santos, W. Schmickler, The pre-exponential factor in electrochemistry, Angew. Chem. Int. Ed. 57 (2018) 7948–7956.
[35] G. Rolando, G.C. Richard, M.F. Juan, G. Eliezer, L. Jacek, S. Wolfgang, T. Sergio, Defining the transfer coefficient in electrochemistry: an assessment (IUPAC technical report), Pure Appl. Chem. 86 (2014) 245–258.
[36] J.A. Christiansen, W.G. Frankenburg, V.I. Komarewsky, E.K. Rideal, The elucidation of reaction mechanisms by the method of intermediates in quasi-stationary concentrations, in: Advances in Catalysis, 5, Academic Press, 1953, pp. 311–353.
[37] E.L. King, C. Altman, A schematic method of deriving the rate laws for enzyme–catalyzed reactions, J. Phys. Chem. 60 (1956) 1375–1378.
[38] S. Kozuch, Steady state kinetics of any catalytic network: graph theory, the energy span model, the analogy between catalysis and electrical circuits, and the meaning of "mechanism", ACS Catal. 5 (2015) 5242–5255.
[39] F. Abild-Pedersen, J. Greeley, F. Studt, J. Rossmeisl, T.R. Munter, P.G. Moses, E. Skúlason, T. Bligaard, J.K. Nørskov, Scaling properties of adsorption energies for hydrogen-containing molecules on transition-metal surfaces, Phys. Rev. Lett. 99 (2007) 016105.
[40] Y. Zhang, J. Zhang, J. Huang, Potential-dependent volcano plot for oxygen reduction: mathematical origin and implications for catalyst design, J. Phys. Chem. Lett. 10 (2019) 7037–7043.
[41] J. Rossmeisl, Z.W. Qu, H. Zhu, G.J. Kroes, J.K. Nørskov, Electrolysis of water on oxide surfaces, J. Electroanal. Chem. 607 (2007) 83–89.
[42] S. Divanis, T. Kutlusoy, I.M. Ingmer Boye, I.C. Man, J. Rossmeisl, Oxygen evolution reaction: a perspective on a decade of atomic scale simulations, Chem. Sci. 11 (2020) 2943–2950.
[43] J.D. Michael, E.L. Demeter, S.M. Illes, Q. Fan, J.R. Boes, J.R. Kitchin, Alkaline electrolyte and fe impurity effects on the performance and active-phase structure of NiOOH thin films for OER catalysis applications, J. Phys. Chem. C 119 (2015) 11475–11481.
[44] A.C. Garcia, T. Touzalin, C. Nieuwland, N. Perini, M.T.M. Koper, Enhancement of oxygen evolution activity of nickel oxyhydroxide by electrolyte alkali cations, Angew. Chem. Int. Ed. 58 (2019) 12999–13003.
[45] X. Zhu, J. Huang, Modeling electrocatalytic oxidation of formic acid at platinum, J. Electrochem. Soc. 167 (2019) 013515.
[46] L.G. Austin, Tafel slopes for flooded diffusion electrodes, Trans. Faraday Soc. 60 (1964) 1319–1324.
[47] M.L. Perry, J. Newman, E.J. Cairns, Mass transport in gas-diffusion electrodes: a diagnostic tool for fuel-cell cathodes, J. Electrochem. Soc. 145 (1998) 5–15.
[48] R.L. Doyle, I.J. Godwin, M.P. Brandon, M.E.G. Lyons, Redox and electrochemical water splitting catalytic properties of hydrated metal oxide modified electrodes, Phys. Chem. Chem. Phys. 15 (2013) 13737–13783.
[49] I.C. Man, H.Y. Su, F. Calle-Vallejo, H.A. Hansen, J.I. Martínez, N.G. Inoglu, J. Kitchin, T.F. Jaramillo, J.K. Nørskov, J. Rossmeisl, Universality in oxygen evolution electrocatalysis on oxide surfaces, ChemCatChem 3 (2011) 1159–1165.
[50] J.T. Feaster, C. Shi, E.R. Cave, T. Hatsukade, D.N. Abram, K.P. Kuhl, C. Hahn, J.K. Nørskov, T.F. Jaramillo, Understanding selectivity for the electrochemical reduction of carbon dioxide to formic acid and carbon monoxide on metal electrodes, ACS Catal. 7 (2017) 4822–4827.
[51] E.L. Clark, S. Ringe, M. Tang, A. Walton, C. Hahn, T.F. Jaramillo, K. Chan, A.T. Bell, Influence of atomic surface structure on the activity of Ag for the electrochemical reduction of CO_2 to CO, ACS Catal. 9 (2019) 4006–4014.
[52] S. Ringe, C.G. Morales-Guio, L.D. Chen, M. Fields, T.F. Jaramillo, C. Hahn, K. Chan, Double layer charging driven carbon dioxide adsorption limits the rate of electrochemical carbon dioxide reduction on Gold, Nat. Commun. 11 (2020) 33.
[53] M. Dunwell, W. Luc, Y. Yan, F. Jiao, B. Xu, Understanding surface-mediated electrochemical reactions: CO_2 reduction and beyond, ACS Catal. 8 (2018) 8121–8129.
[54] L.D. Chen, M. Urushihara, K. Chan, J.K. Nørskov, Electric field effects in electrochemical CO_2 reduction, ACS Catal. 6 (2016) 7133–7139.
[55] D. Bohra, I. Ledezma-Yanez, G. Li, W. de Jong, E.A. Pidko, W.A. Smith, Lateral adsorbate interactions inhibit HCOO− while promoting CO selectivity for CO_2 electrocatalysis on silver, Angew. Chem. Int. Ed. 58 (2019) 1345–1349.
[56] L. Zhang, J. Huang, Understanding surface charge effects in electrocatalysis. Part I: peroxodisulfate reduction at Pt(111), J. Phys. Chem. C 124 (2020) 16951–16960.
[57] M.C. Henstridge, C. Batchelor-McAuley, R. Gusmão, R.G. Compton, Marcus–Hush–Chidsey theory of electron transfer to and from species bound at a non-uniform electrode surface: theory and experiment, Chem. Phys. Lett. 517 (2011) 108–112.
[58] M.C. Henstridge, E. Laborda, N.V. Rees, R.G. Compton, Marcus–Hush–Chidsey theory of electron transfer applied to voltammetry: a review, Electrochim. Acta 84 (2012) 12–20.